Journal of Power Sources Advances 15 (2022) 100090

Contents lists available at ScienceDirect

Journal of Power Sources Advances

journal homepage: www.sciencedirect.com/journal/journal-of-power-sources-advances

Tuning the photocatalytic properties of porphyrins for hydrogen evolution reaction: An in-silico design strategy

Cleber F.N. Marchiori [a,*], Giane B. Damas [b,**], C. Moyses Araujo [a,c,***]

[a] Department of Engineering and Physics, Karlstad University, 65188, Karlstad, Sweden
[b] Department of Physics, Chemistry and Biology, Linköping University, 58330, Linköping, Sweden
[c] Materials Theory Division, Department of Physics and Astronomy, Uppsala University, Box 516, 75120, Uppsala, Sweden

ARTICLE INFO

Keywords:
Photocatalysis
Hydrogen evolution reaction
Donor-acceptor architecture
Porphyrins
Density functional theory

ABSTRACT

Porphyrins constitute a class of attractive materials for harvesting sunlight and promote chemical reactions following their natural activity for the photosynthetic process in plants. In this work, we employ an in-silico design strategy to propose novel porphyrin-based materials as photocatalysts for hydrogen evolution reaction (HER). More specifically, a set of meso-substituted porphyrins with donor-acceptor architecture are evaluated within the density functional theory (DFT) framework, according to these screening criteria: i) broad absorption spectrum in the ultraviolet–visible (UV–Vis) and near infrared (NIR) range, ii) suitable redox potentials to drive the uphill reaction that lead to molecular hydrogen formation, iii) low exciton binding free energy (E_b), and iv) low hydrogen binding free energy (ΔG_H), a quantity that should present low HER overpotentials, ideally $\Delta G_H = 0$. The outcomes indicate that the Se-containing compound, where the donor ligands are attached to the porphyrin core by the spacer, outstands as the most promising candidate that is presented in this work. It displays a broad absorption in the visible and NIR regions to up to 1000 nm, suitable catalytic power, low E_b (in special in high dielectric constant environment, such as water) and the lowest $\Delta G_H = +0.082$ eV. This is comparable, in absolute values, to the value exhibited by platinum ($\Delta G_H = -0.10$ eV), one of the most efficient catalysts for HER.

1. Introduction

The use of solar energy to produce renewable fuels is undoubtedly a promising strategy to supply the current and future demand for a sustainable energy source. Among the solar fuels, hydrogen stands out as one of the cleanest options as no pollutants are produced when it is burned but only water. For this purpose, photocatalysts capable of harvesting photons in a broad range of the solar emission spectrum are desired. Organic materials are natural candidates for this application as nature itself uses organic molecules in the process of solar-to-chemical energy conversion in the photosynthetic processes. Besides that, organic materials have the great advantage of enabling an easier functionalization when compared to inorganic counterparts opening the possibility of tailoring the desired properties [1–4].

In the latest years, a variety of organic photocatalysts for H_2 evolution reaction (HER) have been reported, from molecular [5–7] and polymeric materials [1,8–13] to complex 2-dimensional structures as covalent organic frameworks [14–17] and microporous polymers [18–20]. In particular, copolymers with the donor-acceptor (D-A) configuration have revealed to be active photocatalysts for H_2 production, in particular those containing benzothiadiazole as an acceptor building-block [21–25].

Porphyrins are also a class of attractive materials for driving uphill chemical reactions as they are the main solar energy harvesting compounds that are responsible for the natural photosynthesis. Several porphyrin derivatives have been reported as light absorbing material for photon-to-electricity energy conversion in dye-sensitized solar cells [26] [–] [31] and organic photovoltaic devices [32–38], as well as for photocatalytic HER [14,39–42]. In particular, Cao and co-workers have reported a water-soluble porphyrin derivative for HER from salt water, having platinum as co-catalyst [43]. However, some of those porphyrin derivatives are asymmetric [30,31,44,45] requiring more complex

* Corresponding author.
** Corresponding author. Department of Engineering and Physics, Karlstad University, 65188, Karlstad, Sweden.
*** Corresponding author.
E-mail addresses: cleber.marchiori@kau.se (C.F.N. Marchiori), giane.benvinda.damas@liu.se (G.B. Damas), moyses.araujo@kau.se (C.M. Araujo).

https://doi.org/10.1016/j.powera.2022.100090
Received 18 October 2021; Received in revised form 23 February 2022; Accepted 27 February 2022
Available online 12 March 2022
2666-2485/© 2022 The Authors. Published by Elsevier Ltd. This is an open access article under the CC BY license (http://creativecommons.org/licenses/by/4.0/).

synthetic strategies.

Here, we propose a set of symmetric meso-substituted porphyrins for HER containing the combination of electron rich and electron withdrawing moieties that confer the D-A character to the final compound. Our theoretical assessment of the optical properties show that the substituted porphyrins have a broad absorption spectrum covering all the visible and near infrared (NIR) range of the electromagnetic spectrum, being suitable materials for solar energy harvesting. The calculated reduction potentials reveal that all the proposed compounds have a suitable catalytic power to drive the uphill HER. Moreover, the Se containing compounds display lower exciton binding energies as well as lower hydrogen binding free energy, indicating that, in those materials, the absorption of photons leading to a weakly bound excitons and the incoming protons is not so tightly attached, which facilitates the HER.

2. Computational Details

The optical-related properties of the porphyrin-derivatives and the thermodynamic aspects of the hydrogen evolution reaction (HER) were theoretically assessed by means of time-independent and time-dependent density functional theory (DFT/TD-DFT) [46] frameworks as implemented in Gaussian 16 [47]. The level of theory was set based on the benchmark study that we have previously reported, [4] where M06 [48] was found to be a reliable exchange-correlation functional to reproduce experimental results from cyclic voltammetry and UV–Vis absorption spectroscopy for organic conjugated materials containing similar acceptor units. More specifically, the 6-31G(d) basis set was employed for geometry optimizations and frequency analysis, whereas further single-point calculations (SP) were carried out with the 6-311G (d,p) basis set in accordance with the benchmark report [4,49].

2.1. The photocatalytic cycle: optical and electrochemical properties

In the photocatalytic cycle involving the porphyrin-derivatives as the light harvesting materials (see Scheme 1), the photons from the incident light source are absorbed by the D-A porphyrin (P) forming a bound electron-hole pair known as the *exciton*. This molecule in its excited state (P*) is reduced by an electron donor (II) to subsequently catalyze the H_2 formation (III) (see the left-hand cycle in Scheme 1). This sequence shall be here referred as Path A. Another possibility is P* directly driving the HER (IIa) and being, in sequence, reduced by the electron donor (IIIa) to recover the photocatalyst ground-state (right-hand cycle in Scheme 1). This sequence shall be here referred as Path B. For further details, see Ref. [2].

The UV–Vis absorption spectrum was obtained through TD-DFT calculations (SP) by considering the first 60 singlet electronic transitions along with their respective oscillator strengths, in which the first-transition energy is taken as the optical gap, E_{opt}. This analysis is important to establish whether the material can harvest light in the spectral region of interest, namely the UV-Vis and NIR region (~400-1000 nm), and the extension of such adsorption.

The formation of the photoexcited species P^* was reproduced by calculating E_{opt}. It is worth to remember that E_{opt} is not equal to the fundamental energy gap E_{fund}, as determined through the difference between the oxidation and reduction potentials, because the electrostatic attraction held by the exciton alters the first-excited energy level, usually moving it downward [50,51]. Therefore, the exciton binding energy E_b could be estimated through the difference between these quantities, *i.e.* [52].

$$E_b = E_{fund} - E_{opt}. \quad (1)$$

It is common in the literature to approximate the oxidation and reduction potentials by the frontier orbital energies based on the Koopman's theorem or through vertical transition approximations. These approaches lead to particularly poor description of the reduction potential [4,49]. Thence, we carefully assessed these quantities using the full Gibbs free energies. Furthermore, for the adiabatic exciton binding energy, the excited state was also relaxed to obtain the E_{opt} in the geometry of the first excited state. The effects of different degrees of approximation have also been estimated (see the attached file).

The electrochemical potentials were thus obtained through the reduction reaction free energies, in the solvated environment $\Delta_r G_{(solv)}$, such as (in V)

$$\varphi = -\frac{\Delta_r G_{(solv)}}{nF}, \quad (2)$$

where F and n are the Faraday constant (23.06 kcal mol^{-1} V^{-1}) and the

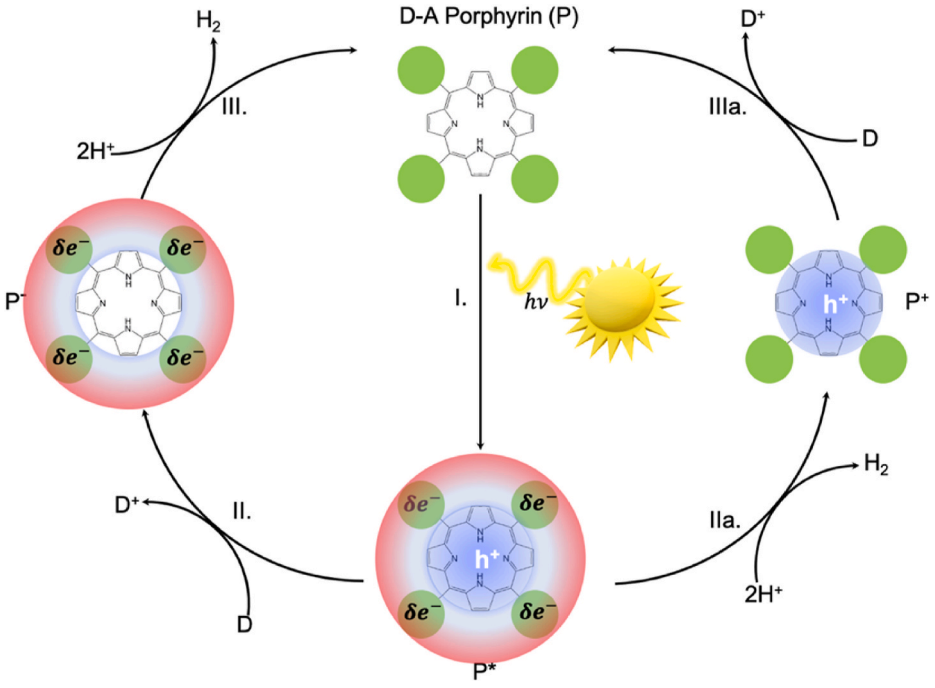

Scheme 1. Diagram representing the possible pathways for the photocatalytic hydrogen evolution, which is triggered by the photon absorption (I), followed by the excited state reduction by some sacrificial agent (electron donor, D) (II) and the sequential H_2 evolution, or the direct H_2 evolution after the excitation (IIa) and the material's recovery by electron transfer from the donor afterwards. The initial material is represented by P, whereas P*, P^-, and P^+ stand for excited, reduced, and oxidized polymer, respectively.

number of electrons involved in the redox reaction, respectively. The oxidation (φ_{ox}) and reduction (φ_{red}) potentials of the porphyrins in their ground-states have been obtained from the free energies of the reactions $P^+ + 1e^- \rightarrow P$ and $P + 1e^- \rightarrow P^-$, respectively. Whereas the oxidation (φ^*_{ox}) and reduction (φ^*_{red}) potentials of the porphyrins in their first-excited states have been obtained from the free energies of the reactions $P^+ + 1e^- \rightarrow P^*$ and $P^* + 1e^- \rightarrow P^-$, respectively. Furthermore, $\Delta_r G_{(solv)}$ was evaluated using the Born-

Haber thermodynamic cycle, as follows:

$$\Delta_r G_{(solv)} = \Delta_r G_{(g)}(Red) + \Delta G_{(solv)}(Red) - \Delta G_{(solv)}(ox), \quad (3)$$

in which

$$\Delta_r G_{(g)}(Red) = \Delta U_{(g)}(red) + PV - T\Delta S_{(g)}(red). \quad (4)$$

In Eq. (3), the solvation free energy of the oxidized and reduced species, $\Delta G_{(solv)}$ *(Ox)* and $\Delta G_{(solv)}$*(Red)*, respectively, were calculated using the polarizable continuum model (SMD) [53] to represent the aqueous environment with dielectric constant $\varepsilon = 78.35$ [54]. Additionally, acetonitrile ($\varepsilon = 35.69$) [55], 1- heptanol ($\varepsilon = 11.32$) [56], acetic acid ($\varepsilon = 6.25$) [47] and thiophene ($\varepsilon = 2.73$) [47] solvent models were considered in this work. The latter solvent is particularly interesting because it gives an approximated value for the dielectric constant related to the organic conjugated polymers and molecules, which is commonly ~3. In Eq. (4), $\Delta U_{(g)}$ and $\Delta S_{(g)}$ stand for internal energy and entropic contributions, respectively. The pressure-volume ($PV = K_bT$) term completes the description of the Gibbs free energy of reaction in gas phase, $\Delta_r G_{(g)}$*(red)*. More specifically, the internal energy of each molecular species in gas phase U was calculated as

$$U = E_{total} + E_{ZPE} + U_{298}, \quad (5)$$

where E_{total} and E_{ZPE} stand for total and zero-point energy, respectively. The last term in Eq. (5) corresponds to the finite temperature contributions at 298 K, also including the statistical mechanics contributions given by vibrational, rotational and translational components. Similarly, such thermal contributions were accounted for in the calculation of the entropy S_{298} to compose the Gibbs Free energy of each species G.

In other words, the photocatalyst is described by the relevant redox levels that are involved in each process step. For instance, the photo-excited species P^* could be reduced immediately by an appropriate electron donor to form the negatively charged species P^-, a step that is represented by the P^*/P^- redox pair, with potential φ^*_{red}. The hole consumption leads to the exciton dissociation, [50] which allows the formation of negatively charged molecule whose relevant redox potential (φ_{red}) is associated to the P/P^- redox pair. Thus, the charge carrier has its thermodynamic driving force increased before it falls into the (H^+/H_2) redox level to form molecular hydrogen as the final product. An alternative pathway involves the P^*/P^+ and P^+/P redox pairs (with potentials φ^*_{ox} and φ_{ox}, respectively) with the reaction-product being formed ahead of the hole consumption [8,50,51,57].

For design purposes, it is also relevant to compute the catalytic power (CP_r) held by the photocatalyst, as it indicates whether the thermodynamic driving force promotes the electron transfer necessary for product formation, namely [1,58].

$$CP_r = \left|\varphi_{red} - \varphi_{H^+/H_2}\right| \quad (6)$$

or

$$CP_r = \left|\varphi^*_{ox} - \varphi_{H^+/H_2}\right|, \quad (7)$$

for paths A and B, respectively.

2.2. Hydrogen binding free energy

The hydrogen binding free energy ΔG_H has been widely pointed out as the main descriptor for HER [1,3,4]. Thus, in order to evaluate the nitrogen and carbon catalytic sites at different porphyrin-derivatives, this quantity was computed through the relation

$$\Delta G_H = G_{porph:H} - \left(G_{porph} + \frac{1}{2}G_{H_2}\right), \quad (8)$$

where $G_{porph:H}$, G_{porph} and G_{H_2} are the Gibbs free energies of the hydrogenated porphyrin-derivative, pristine porphyrin and hydrogen molecule, respectively. The data was obtained in gas phase but also considering the solvation effects in aqueous medium.

3. Results and discussion

3.1. optical aspects

As depicted in Fig. 1 (a), we have investigated a set of six meso-substituted porphyrins as candidate photocatalysts for HER. More precisely, we have evaluated the effect of replacing the sulfur heteroatom in the benzothiadiazole (BT), which is named as 1S – 3S unit by selenium (BSe), resulting in 1Se – 3Se, the insertion of the ethynyl spacer (1 → 2) and also the substitution of the thiophene (T) donor moiety by 3-methylthieno[3,2-b]-thiophene (TT, corresponding to the 2 → 3), which has a more extended π-conjugated structure.

Solution processed asymmetric porphyrin containing benzothiadiazole-thiophene (BT-T) units and the BT-T unit linked to the core by an ethynyl group was already proposed as a way to make the whole molecule planar so that it becomes π-conjugated [59]. Additionally, the push–pull property of the porphyrin core and BT moieties can result in an internal charge transfer (ICT) upon excitation as observed in D-A like molecules. Interestingly, they only observed a broadening on the absorption spectrum for the ethynyl-bridged porphyrin while for the case where the BT-T unit is directly linked to the core, they observe the characteristic spectrum of porphyrins with a well-defined Soret band and the characteristic Q bands [59].

As shown in Fig. 1 (b)–(d), all the calculated absorption spectra displayed a broad absorption spectrum up to 800 nm for the 1S and 1Se (see Fig. 1 (b)), which is further extended to the NIR region when the extended π-conjugated unit and spacer is inserted (see Fig. 1 (c) and (d)). All the contribution for the electronic transitions and the oscillator strengths are displayed in Table S1 in the Supporting Information file. In all cases, the dual (or multiple) band feature was observed where the Q-bands are not possible to resolve. This is a strong indication that the ICT character is achieved thanks to the presence of both electron-rich units, such as the T and TT, and electron-withdrawing units as BT(BSe).

It is possible to see in Fig. 2 where the spatial distribution of the frontier orbitals for the Se containing molecules are presented (for the S series' orbital, see Fig. S1 in the supporting information file). For both 1S and 1Se systems, the HOMO orbital is delocalized over the whole molecules while the LUMO is more localized at the acceptor units, *viz.* The BT/BSe and the porphyrin core. The insertion of the ethynyl spacer, which result in the molecules 2S and 2Se, along with the replacement of T by TT (resulting in 3S and 3Se) promoted the distribution of the HOMO extending from the core to the T/TT units nearby. Although these substitutions keep the same characteristics of the LUMO (localization at the acceptor units) as for 2S and 2Se, in the TT containing molecules the LUMO distribution at the BT units are decreased being more localized at the porphyrin core. This charge separation effect has an impact on the electron-hole coulombic interaction, reducing the exciton binding energy as will be discussed later.

To evaluate the effect of the charge reorganization upon reduction or oxidation, induced by structural relaxation in the charged states, Fig. 2 also displays the cation and anion spin densities. It is possible to see that for all the molecules, the cation spin distribution follows the HOMO spatial distribution, indicating that the relaxation upon oxidation has a minor impact on the charge redistribution. Similar effect was observed

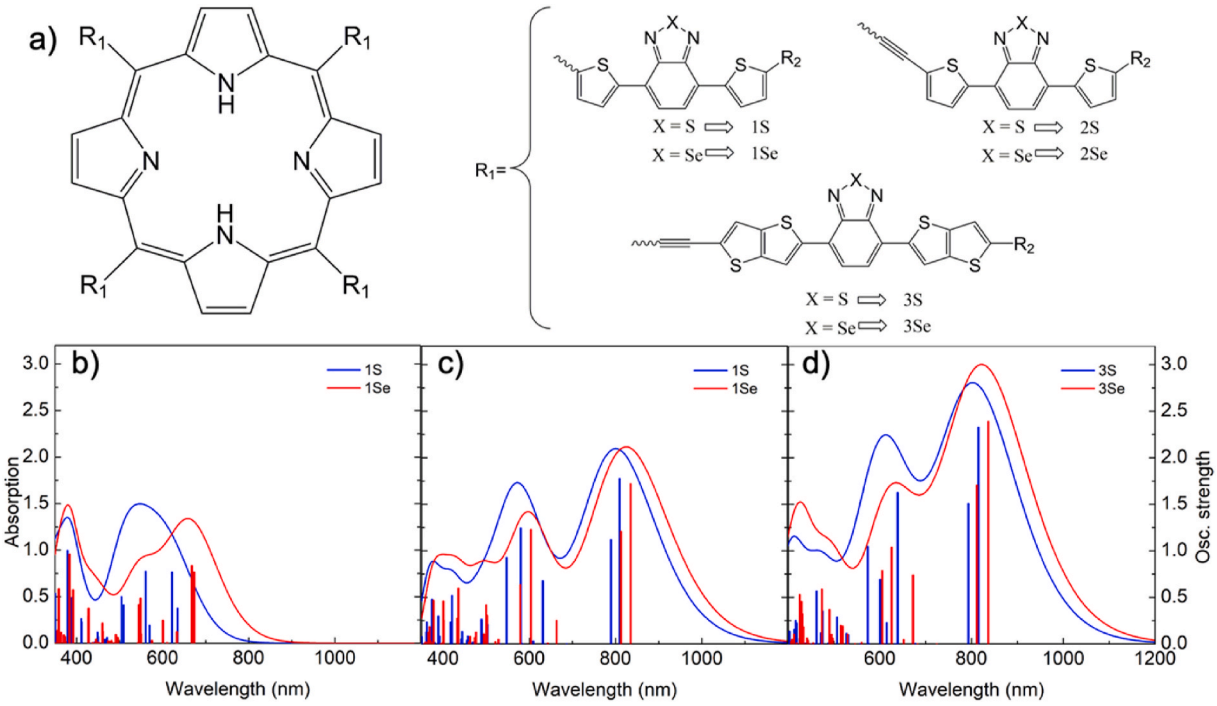

Fig. 1. a) Molecular structures of the compounds that are discussed in this study. The original alkyl chains have been replaced by methyl groups, as indicated by R2. Comparison of calculated absorption spectra for b) 1S and 1Se, c) 2S and 2Se and d) 3S and 3Se. The spectra were obtained from TD-DFT calculation at M06/6-311G (d,p) theory level.

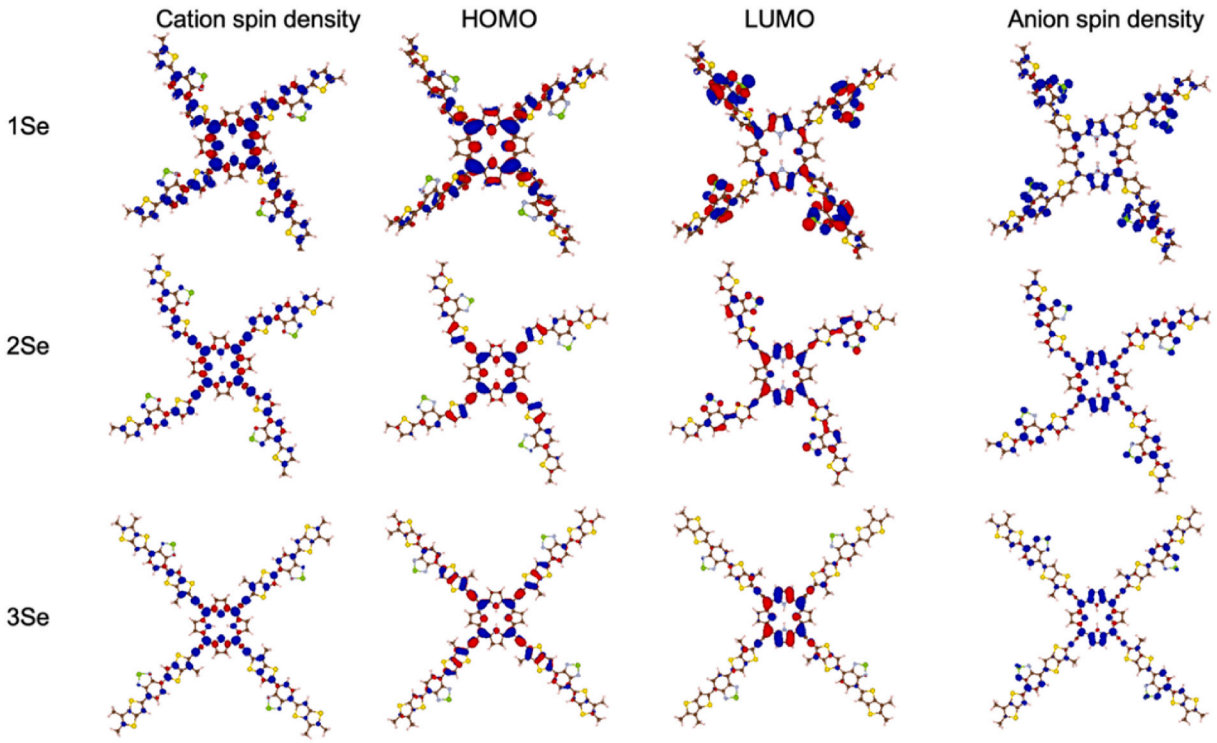

Fig. 2. Comparison between the cation and anion spin density and the spatial distribution of the ground-state HOMO and LUMO orbital for the Se containing compounds. Both orbitals and spin densities were calculated at M06/6-311G(d,p) theory levels (isosurfaces = 0.02 for HOMO and LUMO orbitals and isosurfaces = 0.001 for the spin densities).

for the reduction, except for 3Se (and similarly for 3S as shown in Fig. S1 in the supporting information file), which displayed a spin distribution over the BT/BSe units that is not seen in the LUMO distribution. As the molecules in their reduced or excited state will drive the uphill reaction, the anion spin densities reveal that both the porphyrin core and the BT/BSe units can act as the catalytic sites for HER. In previous works we have investigated the BT/BSe units as catalytic sites when employed as acceptor moiety in both copolymer and symmetric small-molecules, [2]

[–] [4] having its performance also experimentally validated [1]. Following this line, we focus our investigation on the substituent, letting the exploration of the porphyrin core as catalytic site as the scope of a future work.

3.2. Thermodynamic aspects

As explained in Section 2.1 in the Computational Details, the catalytic power CP_r is an important property to determine whether the thermodynamic condition necessary for product formation is satisfied, a quantity that is calculated by subtracting the proton redox potential φ_{H^+/H_2} from the potentials of the P/P^- or P^*/P^+ redox pairs, depending on the reaction pathway considered in Scheme 1. Fig. 3 (a) and (b) show the calculated redox potentials for both ground and excited states. The reduction potentials φ_{red} and the excitonic oxidation potentials φ^*_{ox} correspond to the catalytic power as described by eqs. (6) and (7). All porphyrin-derivatives of interest in this work exhibit catalytic power for HER, with calculated values ranging from 0.75 to 1.45 V and 0.27–0.80 V in thiophene and water solvent environment, respectively when path A is considered. For path B, when the excited state drives the HER, the CP_r is in the range of 0.31–0.62 V in low dielectric environment (thiophene) and 0.46–0.85 V in water, considering all the thermal contributions to the Gibbs free energy of the excited state.

Nonetheless, each substitution represented by (x→y) plays a different role on this property, as it is further discussed. All variations in potential (Δd) cited below are given in reference to the standard hydrogen electrode (SHE) and discussed in detail for the cases where thiophene ($\varepsilon = 2.72$) or water ($\varepsilon = 78.35$) are considered as dielectric environment.

Firstly, including the ethynyl group to connect the porphyrin core with its ligands in 2(S/Se) compounds leads to a significant decrease in catalytic power for HER (1S/Se→2S/Se). For instance, φ_{red} decreases from −1.3 to −0.8 V (Δd = +0.5 V) and from −1.5 to −0.8 V (Δd = +0.7 V) for S- and Se-based compounds, respectively, in thiophene environment (see Fig. 3 (a)). Similar values are found in water environment, with Δd = +0.4 and + 0.8 eV, respectively. On the other hand, the (P^+/P) redox potential is barely affected by this modification in 1S→2S, but becomes more positive in ~0.45 V for Se-based compounds regardless of the solvent. In addition, the decreased E_{fund}, *i.e.,* the energy difference between φ_{red} and φ_{ox}, leads to a smaller E_b (~0.15 eV) upon addition of the ethynyl group in comparison with 1 independently of the heteroatom or solvent.

The replacement of T by TT (2 → 3) has no significant effect over the ground state catalytic power of 2S/3S in either solvent, whereas it raises slightly (Δd~ 0.1–0.2 V) for Se-based compounds. The former porphyrins have φ_{ox} decreased in 0.2–0.3 V, but there is some increase in Δd = 0.2 V for (2Se→3Se). The overall effect on E_b is quite small in either case.

Both ground-state potentials φ_{ox} and φ_{red} as well as the oxidation (φ^*_{ox}) and reduction (φ^*_{red}) potentials of the porphyrins in their first-excited states have been obtained from the free energies of the reaction. The calculations were performed at M06/6-311G(d,p) theory level. (c) The adiabatic exciton binding energy E_b considering different dielectric constants for the calculations.

When the compounds 1 and 3 are compared, the significant decrease in catalytic power (Δd = 0.5/0.7 V for S/Se compounds) is mainly caused by the inclusion of the ethynyl group, as explained before. The φ_{ox} has significant decrease from 0.3 to 0.4 V for S/Se porphyrins. Therefore, E_b also diminishes in 0.1–0.2 eV in connection with the decreased E_{fund}.

Finally, the heteroatom substitution (S→Se) does not lead to drastic alterations to the redox potentials and, consequently, E_{fund} and E_b are barely affected by such replacement. For instance, the thermodynamic driving force for electron or hole transfer for 1 (1S → 1Se) remains unaltered in thiophene but increases in ~0.15 V in water environment, similarly to the behavior shown by 3 (3S → 3Se) for the hole transfer in water. Here, it is interesting to notice that the large decrease in redox potential for 2 (2S → 2Se) in 0.3 V is compensated by the increased optical gap, leading to an unaffected exciton binding free energy upon heteroatom substitution.

One interesting feature regarding the E_b appears when different

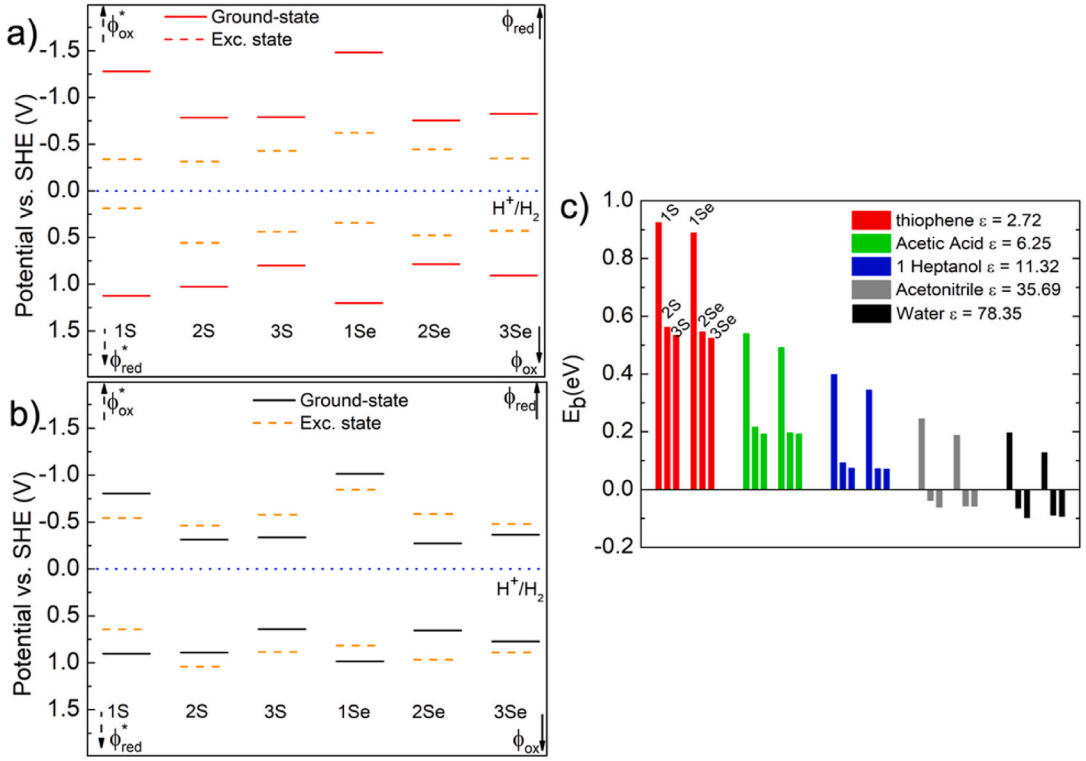

Fig. 3. Ground-state (GS) and excited state redox potentials in thiophene (a) and water (b).

solvents, with different dielectric constants, are considered. As plotted in Fig. 3 (c), the E_b is drastically reduced as the dielectric constant of the continuum medium, used to compute the solvation free energy, increases. This feature is similar in the vertical approach when no relaxation effects are considered and when the relaxation of both ionic and excited states are taken into account to compose an adiabatic binding energy and even when all the thermal contributions to the Gibbs free energy are considered (see Table S2 in the Supporting Information file). For the thiophene, which has the lowest value of $\varepsilon = 2.72$ amongst the solvents considered in our study, the vertical E_b are in the range 500 meV–600 meV while the adiabatic E_b are in the range 500 meV–900 meV, clearly showing the effect of the molecular relaxation in the excited state. That regime mimics the case where the molecules are aggregated or forming a thin film, as the dielectric constant for organic conjugated materials is known to be low ($\varepsilon \sim 3$). In this case, the excitons formed upon absorption of one photon are tightly bound and the HER or the reduction of the molecule in its excited state requires a fast process to compete with the charge recombination. When the dielectric constant is increased to 6.25, which is the case of acetic acid, E_b decreases to values between 150 meV (190 meV) to 310 meV (550 meV) in vertical (adiabatic) approaches, and further increasing ε to 11.32, in the case of 1-heptanol, the E_b drop to values as low as 30 meV (73 meV) (the range for E_b in this case is 30 (73 meV) – 160 meV (400 meV)). It is worth to highlight that in all the cases, the insertion of the spacers and the TT units promote a substantial decrement in E_b thanks to the more pronounce internal charge transfer observed for these materials, as discussed before, and also observed in the orbital spatial distributions, shown in Fig. 2. The extreme case is observed when high values of dielectric constants are considered, *viz.* when acetonitrile or water are used to compute the solvation free energy. For these cases, the E_b assume negative values, even in the adiabatic regime, indicating that the photon absorption leads directly to the formation separated charges stabilized by the dielectric environment. This corresponds to the case where the molecules are either soluble in those solvents and can be well dispersed in them, or when forming porous networks or nanostructures where the surface area is increased and thus both optical and electrochemical processed are more surface dependent being strongly influenced by the solvent. In this case, the recombination processes are expected to be disfavored as the unbound charges are spatially separated and screened by the solvation effects. Thus, the slow rate proton coupled reaction can take place effectively. This result is one more evidence of the promising features of these meso-substituted porphyrins as photocatalysts for HER. In our calculations, we also considered all the thermal contributions to the Gibbs free energy of the excited state. We observed just a small variation when only the relaxation is taken into account, showing that, at least for the molecules discussed in this work, the thermal contributions play a minor role. For the numeric values, please see Table S2 in the Supporting Information file.

3.3. Hydrogen binding free energy

The hydrogen binding free energy (ΔG_H), depicted in Fig. 4, is another relevant individual factor for design purposes in HER photocatalysis. The choice of adsorption site lies in the presence of electron density upon photoexcitation, namely the spin density localization, as well as its ability to bind the hydrogen atom [1,4,49,60]. In this sense, we previously demonstrated that S- and Se-sites exhibit higverpotentials for HER in benzothiadiazole-containing copolymers, [1,4,49] thus being unfeasible as the catalytic sites in related materials. Thence, we herein consider nitrogen and carbon atoms for such purpose, based on previous assessment in polymeric materials [1,4,49,60,61]. The values for ΔG_H summarized in Table 1 were obtained at the M06/6-311G(d,p) level of theory, where the basis set was adjusted in a stepwise procedure, *i.e.* the optimization and frequency calculations were performed using the 6-31G(d) basis set, followed by a single-point step at the 6-311G(d,p) level to compose the Gibbs free energy of each species.

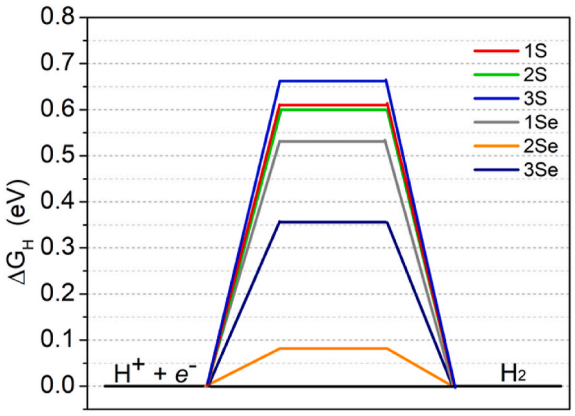

Fig. 4. Hydrogen binding free energies (ΔG_H) calculated at the nitrogen catalytic site for the S- and Se-based porphyrins studied in this work.

Table 1
Binding Free Energies (in eV) obtained in gas phase and aqueous environment. Level of theory: M06/6-311G(d,p). Solvation method: SMD. Note: The boldface values indicate the values for the most outstanding material in this work.

System	ΔG_H(g)		ΔG_H(solv)	
S derivatives	N-site	C-site	N-site	C-site
1S	+0.664	+0.363/0.335	+0.610	+0.342/0.317
2S	+0.650	+0.434/0.469	+0.600	+0.424/0.471
3S	+0.739	+0.464/0.393	+0.662	+0.461/0.400
Se derivatives				
1Se	+0.589	+0.589/0.575	+0.531	+0.578/0.570
2Se	**+0.125**	**+0.302/0.303**	**+0.082**	**+0.300/0.313**
3Se	+0.430	+0.296/0.287	+0.356	+0.304/0.307

In general, the low values for $\Delta G_H = 0.300$–0.570 eV in the C-site demonstrate its feasibility as a potential catalytic site for photocatalytic purposes, as verified for poly(p-phenylene) by Prentice et al. [60,61] For the N-site, the BT unit offers ΔG_H varying from +0.600 to +0.662 eV for S-compounds, a range that is significantly decreased with the heteroatom substitution (S →Se), with $\Delta G_H = +0.082$ to +0.531 eV. These values are in agreement with our previous contributions, where BT was used as electron-withdrawing unit in the fluorene-thiophene-based copolymer [1,4]. Moreover, the 2Se porphyrin displayed an outstanding value for $\Delta G_H = +0.082$ eV, which is comparable, in absolute values, with that displayed for platinum (= −0.10 eV) [62].

Finally, it is worth to mention that the some works attribute the photocatalytic activity of organic materials to the residual metals such as palladium used as catalysts during the synthesis [63,64]. However, some of us in a joint experimental/theoretical study reported recently a small organic molecule based on the benzothiadiazole unit, preparade without the use of metallic catalyst and still having a considerable activity as electrocatalyst for hydrogen production [65]. This result ensures the capability of organic materials as photo(electro)catalysts for HER.

4. Conclusions

In summary, we have investigated a set of meso-substituted porphyrins containing donor-acceptor-like ligands as candidate materials as photocatalysts for hydrogen evolution reaction. Our strategy, based in an atomistic scale modelling, aims to provide a guidance to a rational design of advanced materials for solar-to-chemical energy conversion. In this sense, we evaluated the effects of inserting D-A groups symmetrically attached to the porphyrin core, which can make the synthetic routes easier. We also investigated the effect of inserting of a spacer and

extension of the thiophene donor moiety, along with the substitution of the sulfur atoms at the benzothiadiazole units by selenium on the absorption profile and the electrochemical potentials. To complete the screening protocol, we computed the exciton binding energies and the hydrogen binding free energies, which is shown to be a good descriptor for the material's performance as photocatalyst. The outcomes showed that all the porphyrins-derivatives indeed displayed a D-A character with the characteristic ICT absorption peak, leading to spatially separated and less bound excitons, in special for the spacer containing compounds. Moreover, if the molecules are possible to solvate or disperse in water, the photon absorption could lead directly to separated charges, which could favor the HER as it is expected to be a low-rate proton coupled type of reaction. All the proposed molecules have an appreciable catalytic power being capable to drive the uphill HER. Amongst the proposed molecules, the 2Se outstands as a very promising material for HER thanks to its broad absorption spectrum, suitable reduction potential leading to an appreciable catalytic power, lowered exciton binding energy (a consequence of the spatial separation of electron-holes pair formed upon optical excitation) and the low hydrogen binding free energy, comparable with one of the most used catalysts, the platinum.

Data availability

The data that supports the findings of this study are available within the article and its supplementary material.

Declaration of interests

The authors declare that they have no known competing financial interests or personal relationships that could have appeared to influence the work reported in this paper.

Acknowledgments

CMA and CFNM acknowledge Swedish Research Council (grant nos. 2014-05984 and 2020-05223), Swedish Energy Agency (grant no. 45420-1) for supporting this project, as well as the Swedish National Infrastructure for Computing (SNIC) at the PDC Center for High Performance Computing and National Supercomputer Centre at Linköping University (NSC) for providing the computational infrastructure. GBD would like to express the sincere gratitude for the financial support provided by CAPES (Coordenação de Aperfeiçoamento de Pessoal de Ensino Superior) during her Phd studies.

Appendix A. Supplementary data

Supplementary data to this article can be found online at https://doi.org/10.1016/j.powera.2022.100090.

References

[1] P.B. Pati, G. Damas, L. Tian, D.L.A.A. Fernandes, L. Zhang, I.B. Pehlivan, T. Edvinsson, C.M. Araujo, H. Tian, An experimental and theoretical study of an efficient polymer nano-photocatalyst for hydrogen evolution, Energy Environ. Sci. 10 (2017) 1372–1376, https://doi.org/10.1039/c7ee00751e.

[2] G.B. Damas, C.F.N. Marchiori, C.M. Araujo, Tailoring the electron-rich moiety in benzothiadiazole-based polymers for an efficient photocatalytic hydrogen evolution reaction, J. Phys. Chem. C 123 (42) (2019) 25531–25542, https://doi.org/10.1021/acs.jpcc.9b06057.

[3] G.B. Damas, F. Von Kieseritzky, J. Hellberg, C.F.N. Marchiori, C.M. Araujo, Symmetric small-molecules with acceptor-donor-acceptor architecture for efficient visible-light driven hydrogen production: optical and thermodynamic aspects, J. Phys. Chem. C 123 (51) (2019) 30799–30808, https://doi.org/10.1021/acs.jpcc.9b07721.

[4] G. Damas, C.F.N. Marchiori, C.M. Araujo, On the design of donor-acceptor conjugated polymers for photocatalytic hydrogen evolution reaction: first-principles theory-based assessment, J. Phys. Chem. C 122 (47) (2018) 26876–26888, https://doi.org/10.1021/acs.jpcc.8b09408.

[5] J. Kosco, M. Bidwell, H. Cha, T. Martin, C.T. Howells, M. Sachs, D.H. Anjum, S. Gonzalez Lopez, L. Zou, A. Wadsworth, W. Zhang, L. Zhang, J. Tellam, R. Sougrat, F. Laquai, D.M. DeLongchamp, J.R. Durrant, I. McCulloch, Enhanced photocatalytic hydrogen evolution from organic semiconductor heterojunction nanoparticles, Nat. Mater. 19 (2020) 559–565, https://doi.org/10.1038/s41563-019-0591-1.

[6] T.J. Whittemore, C. Xue, J. Huang, J.C. Gallucci, C. Turro, Single-chromophore single-molecule photocatalyst for the production of dihydrogen using low-energy light, Nat. Chem. 12 (2020) 180–185, https://doi.org/10.1038/s41557-019-0397-4.

[7] H. Tian, Molecular catalyst immobilized photocathodes for water/proton and carbon dioxide reduction, ChemSusChem 8 (2015) 3746–3759, https://doi.org/10.1002/cssc.201500983.

[8] R.S. Sprick, J.X. Jiang, B. Bonillo, S. Ren, T. Ratvijitvech, P. Guiglion, M. A. Zwijnenburg, D.J. Adams, A.I. Cooper, Tunable organic photocatalysts for visible-light-driven hydrogen evolution, J. Am. Chem. Soc. 137 (9) (2015) 3265–3270, https://doi.org/10.1021/ja511552k.

[9] L. Wang, R. Fernández-Terán, L. Zhang, D.L.A. Fernandes, L. Tian, H. Chen, H. Tian, Organic polymer dots as photocatalysts for visible light-driven hydrogen generation, Angew. Chem. Int. Ed. 55 (2016) 12306–12310, https://doi.org/10.1002/anie.201607018.

[10] A. Liu, C.-W.W. Tai, K. Holá, H. Tian, Hollow polymer dots: nature-mimicking architecture for efficient photocatalytic hydrogen evolution reaction, J. Mater. Chem. A. 7 (2019) 4797–4803, https://doi.org/10.1039/c8ta12146j.

[11] C.M. Aitchison, M. Sachs, M.A. Little, L. Wilbraham, N.J. Brownbill, C.M. Kane, F. Blanc, M.A. Zwijnenburg, J.R. Durrant, R.S. Sprick, A.I. Cooper, Structure–activity relationships in well-defined conjugated oligomer photocatalysts for hydrogen production from water, Chem. Sci. 11 (2020) 8744–8756, https://doi.org/10.1039/D0SC02675A.

[12] Y. Bai, D.J. Woods, L. Wilbraham, C.M. Aitchison, M.A. Zwijnenburg, R.S. Sprick, A.I. Cooper, Hydrogen evolution from water using heteroatom substituted fluorene conjugated co-polymers, J. Mater. Chem. A. 8 (2020) 8700–8705, https://doi.org/10.1039/D0TA02599B.

[13] J. Jayakumar, H.-H. Chou, Recent advances in visible-light-driven hydrogen evolution from water using polymer photocatalysts, ChemCatChem 12 (2020) 689–704, https://doi.org/10.1002/cctc.201901725.

[14] E. Giannoudis, E. Benazzi, J. Karlsson, G. Copley, S. Panagiotakis, G. Landrou, P. Angaridis, V. Nikolaou, C. Matthaiaki, G. Charalambidis, E.A. Gibson, A. G. Coutsolelos, Photosensitizers for H2 evolution based on charged or neutral Zn and Sn porphyrins, Inorg. Chem. 59 (2020) 1611–1621, https://doi.org/10.1021/acs.inorgchem.9b01838.

[15] B.P. Biswal, H.A. Vignolo-González, T. Banerjee, L. Grunenberg, G. Savasci, K. Gottschling, J. Nuss, C. Ochsenfeld, B.V. Lotsch, Sustained solar H2 evolution from a thiazolo[5,4-d]thiazole-bridged covalent organic framework and nickel-thiolate cluster in water, J. Am. Chem. Soc. 141 (2019) 11082–11092, https://doi.org/10.1021/jacs.9b03243.

[16] C.B. Meier, R. Clowes, E. Berardo, K.E. Jelfs, M.A. Zwijnenburg, R. Sebastian Sprick, A.I. Cooper, Structurally diverse covalent triazine-based framework materials for photocatalytic hydrogen evolution from water, Chem. Mater. 31 (2019) 8830–8838, https://doi.org/10.1021/acs.chemmater.9b02825.

[17] P. Pachfule, A. Acharjya, J. Roeser, T. Langenhahn, M. Schwarze, R. Schomäcker, A. Thomas, J. Schmidt, Diacetylene functionalized covalent organic framework (COF) for photocatalytic hydrogen generation, J. Am. Chem. Soc. 140 (2018) 1423–1427, https://doi.org/10.1021/jacs.7b11255.

[18] Z. Wang, X. Yang, T. Yang, Y. Zhao, F. Wang, Y. Chen, J. Hui Zeng, C. Yan, F. Huang, J.-X. Jiang, Dibenzothiophene dioxide based conjugated microporous polymers for visible-light-driven hydrogen production, ACS Catal. 8 (2018) 8590–8596, https://doi.org/10.1021/acscatal.8b02607.

[19] R. Sebastian Sprick, Y. Bai, A.A.Y. Guilbert, M. Zbiri, C.M. Aitchison, L. Wilbraham, Y. Yan, D.J. Woods, M.A. Zwijnenburg, A.I. Cooper, Photocatalytic hydrogen evolution from water using fluorene and dibenzothiophene sulfone-conjugated microporous and linear polymers, Chem. Mater. 31 (2018) 305–313, https://doi.org/10.1021/acs.chemmater.8b02833.

[20] Q.-R. Zeng, Z.-H. Cheng, C. Yang, Y. He, N. Meng, C.F.J. Faul, Y.-Z. Liao, Metal-free synthesis of pyridyl conjugated microporous polymers for photocatalytic hydrogen evolution, Chin. J. Polym. Sci. 39 (2021) 1004–1012, https://doi.org/10.1007/s10118-021-2574-3.

[21] Y. Xu, N. Mao, C. Zhang, X. Wang, J. Zeng, Y. Chen, F. Wang, J.X. Jiang, Rational design of donor-Π-acceptor conjugated microporous polymers for photocatalytic hydrogen production, Appl. Catal. B Environ. 228 (2018) 1–9, https://doi.org/10.1016/j.apcatb.2018.01.073.

[22] E. Lanzarini, M. Rosa Antognazza, M. Biso, A. Ansaldo, L. Laudato, P. Bruno, P. Metrangolo, G. Resnati, D. Ricci, G. Lanzani, Polymer-based photocatalytic hydrogen generation, J. Phys. Chem. C 116 (2012) 10944–10949, https://doi.org/10.1021/jp212107f.

[23] Z.-A. Lan, W. Ren, X. Chen, Y. Zhang, X. Wang, Conjugated donor-acceptor polymer photocatalysts with electron-output "tentacles" for efficient hydrogen evolution, Appl. Catal. B Environ. 245 (2019) 596–603, https://doi.org/10.1016/j.apcatb.2019.01.010.

[24] L. Li, W. Lo, Z. Cai, N. Zhang, L. Yu, Donor–acceptor porous conjugated polymers for photocatalytic hydrogen production: the importance of acceptor comonomer, Macromolecules 49 (2016) 6903–6909, https://doi.org/10.1021/acs.macromol.6b01764.

[25] K. Kailasam, M.B. Mesch, L. Möhlmann, M. Baar, S. Blechert, M. Schwarze, M. Schröder, R. Schomäcker, J. Senker, A. Thomas, Donor–acceptor-type

heptazine-based polymer networks for photocatalytic hydrogen evolution, Energy Technol. 4 (2016) 744–750, https://doi.org/10.1002/ente.201500478.
[26] S. Karthikeyan, J.Y. Lee, Zinc-porphyrin based dyes for dye-sensitized solar cells, J. Phys. Chem. 117 (2013) 10973–10979, https://doi.org/10.1021/jp408473k.
[27] T. Bessho, S.M. Zakeeruddin, C.Y. Yeh, E.W.G. Diau, M. Grätzel, Highly efficient mesoscopic dye-sensitized solar cells based on donor-acceptor-substituted porphyrins, Angew. Chem. Int. Ed. 49 (2010) 6646–6649, https://doi.org/10.1002/anie.201002118.
[28] K. Zeng, Z. Tong, L. Ma, W.-H. Zhu, W. Wu, Y. Xie, Molecular engineering strategies for fabricating efficient porphyrin-based dye-sensitized solar cells, Energy Environ. Sci. 13 (2020) 1617–1657, https://doi.org/10.1039/C9EE04200H.
[29] M. Cariello, S.M. Abdalhadi, P. Yadav, J.-D. Decoppet, S.M. Zakeeruddin, M. Grätzel, A. Hagfeldt, G. Cooke, An investigation of the roles furan versus thiophene π-bridges play in donor–π-acceptor porphyrin based DSSCs, Dalton Trans. 47 (2018) 6549–6556, https://doi.org/10.1039/C8DT00413G.
[30] L. Cabau, C. Vijay Kumar, A. Moncho, J.N. Clifford, N. López, E. Palomares, A single atom change "switches-on" the solar-to-energy conversion efficiency of Zn-porphyrin based dye sensitized solar cells to 10.5%, Energy Environ. Sci. 8 (2015) 1368–1375, https://doi.org/10.1039/C4EE03320E.
[31] S. Fan, K. Lv, H. Sun, G. Zhou, Z.-S. Wang, The position effect of electron-deficient quinoxaline moiety in porphyrin based sensitizers, J. Power Sources 279 (2015) 36–47, https://doi.org/10.1016/j.jpowsour.2014.12.143.
[32] V. Cuesta, M. Vartanian, P. de la Cruz, R. Singhal, G.D. Sharma, F. Langa, Comparative study on the photovoltaic characteristics of A–D–A and D–A–D molecules based on Zn-porphyrin; a D–A–D molecule with over 8.0% efficiency, J. Mater. Chem. A. 5 (2017) 1057–1065, https://doi.org/10.1039/C6TA09408B.
[33] T. Liang, L. Xiao, K. Gao, W. Xu, X. Peng, Y. Cao, Modifying the chemical structure of a porphyrin small molecule with benzothiophene groups for the reproducible fabrication of high performance solar cells, ACS Appl. Mater. Interfaces 9 (2017) 7131–7138, https://doi.org/10.1021/acsami.6b15241.
[34] F. Lu, Y. Feng, X. Wang, Y. Zhao, G. Yang, J. Zhang, B. Zhang, Z. Zhao, Influence of the additional electron-withdrawing unit in β-functionalized porphyrin sensitizers on the photovoltaic performance of dye-sensitized solar cells, Dyes Pigments 139 (2017) 255–263, https://doi.org/10.1016/j.dyepig.2016.12.027.
[35] H. Yin, S. Chen, S.H. Cheung, H.W. Li, Y. Xie, S.W. Tsang, X. Zhu, S.K. So, Porphyrin-based thick-film bulk-heterojunction solar cells for indoor light harvesting, J. Mater. Chem. C. 6 (2018) 9111–9118, https://doi.org/10.1039/c8tc02838a.
[36] H. Yin, J.K.W. Ho, V. Piradi, S. Chen, X. Zhu, S.K. So, Highly-transparent and true-colored semitransparent indoor photovoltaic cells, Small Methods 4 (2020) 2000136, https://doi.org/10.1002/smtd.202000136.
[37] K. Gao, Y. Kan, X. Chen, F. Liu, B. Kan, L. Nian, X. Wan, Y. Chen, X. Peng, T. P. Russell, Y. Cao, A.K.-Y. Jen, Low-Bandgap porphyrins for highly efficient organic solar cells: materials, morphology, and applications, Adv. Mater. 32 (2020) 1906129, https://doi.org/10.1002/adma.201906129.
[38] Y. Guo, A. Zhang, C. Li, W. Li, D. Zhu, A near-infrared porphyrin-based electron acceptor for non-fullerene organic solar cells, Chin. Chem. Lett. 29 (2018) 371–373, https://doi.org/10.1016/j.cclet.2017.08.006.
[39] Y. Zhang, K. Ren, L. Wang, L. Wang, Z. Fan, Porphyrin-based heterogeneous photocatalysts for solar energy conversion, Chin. Chem. Lett. 33 (1) (2021) 33–60, https://doi.org/10.1016/j.cclet.2021.06.013.
[40] P. Zeng, Y. Zheng, S. Chen, H. Liu, R. Li, T. Peng, Asymmetric zinc porphyrin derivatives bearing three pseudo-pyrimidine meso-position substituents and their photosensitization for H2 evolution, New J. Chem. 44 (2020) 11237–11247, https://doi.org/10.1039/D0NJ02056G.
[41] N. Chanda, D. Koteshwar, S. Gonuguntla, S. Bojja, U. Pal, L. Giribabu, Efficient visible-light-driven hydrogen production by Zn–porphyrin based photocatalyst with engineered active donor–acceptor sites, Mater. Adv. 2 (2021) 4762–4771, https://doi.org/10.1039/D1MA00342A.
[42] M. Joseph, S. Haridas, Recent progresses in porphyrin assisted hydrogen evolution, Int. J. Hydrogen Energy 45 (2020) 11954–11975, https://doi.org/10.1016/j.ijhydene.2020.02.103.
[43] X. Yang, Z. Hu, Q. Yin, C. Shu, X.-F. Jiang, J. Zhang, X. Wang, J.-X. Jiang, F. Huang, Y. Cao, Water-soluble conjugated molecule for solar-driven hydrogen evolution from salt water, Adv. Funct. Mater. 29 (13) (2019) 1808156, https://doi.org/10.1002/adfm.201808156.
[44] F. Cheng, X. He, L. Yin, B. Xie, Y. Li, Design and structural modification of narrow-bandgap small molecules based on asymmetric porphyrin-diketopyrrolopyrrole backbone for solution-processed organic solar cells, Dyes Pigments 176 (2020) 108211, https://doi.org/10.1016/j.dyepig.2020.108211.
[45] P.S. Gangadhar, S. Gonuguntla, S. Madanaboina, N. Islavath, U. Pal, L. Giribabu, Unravelling the impact of thiophene auxiliary in new porphyrin sensitizers for high solar energy conversion, J. Photochem. Photobiol. Chem. 392 (2020) 112408, https://doi.org/10.1016/j.jphotochem.2020.112408.
[46] R.E. Stratmann, G.E. Scuseria, M.J. Frisch, An efficient implementation of time-dependent density-functional theory for the calculation of excitation energies of large molecules, J. Chem. Phys. 109 (1998) 8218, https://doi.org/10.1063/1.477483.
[47] M.J. Frisch, G.W. Trucks, H.B. Schlegel, G.E. Scuseria, M.A. Robb, J.R. Cheeseman, G. Scalmani, V. Barone, G.A. Petersson, H. Nakatsuji, X. Li, M. Caricato, A. V. Marenich, J. Bloino, B.G. Janesko, R. Gomperts, B. Mennucci, H.P. Hratchian, J. V. Ortiz, A.F. Izmaylov, J.L. Sonnenberg, D. Williams-Young, F. Ding, F. Lipparini, F. Egidi, J. Goings, B. Peng, A. Petrone, T. Henderson, D. Ranasinghe, V. G. Zakrzewski, J. Gao, N. Rega, G. Zheng, W. Liang, M. Hada, M. Ehara, K. Toyota, R. Fukuda, J. Hasegawa, M. Ishida, T. Nakajima, Y. Honda, O. Kitao, H. Nakai, T. Vreven, K. Throssell, J. Montgomery, J. A, J.E. Peralta, F. Ogliaro, M. J. Bearpark, J.J. Heyd, E.N. Brothers, K.N. Kudin, V.N. Staroverov, T.A. Keith, R. Kobayashi, J. Normand, K. Raghavachari, A.P. Rendell, J.C. Burant, S.S. Iyengar, J. Tomasi, M. Cossi, J.M. Millam, M. Klene, C. Adamo, R. Cammi, J.W. Ochterski, R.L. Martin, K. Morokuma, O. Farkas, J.B. Foresman, D.J. Fox, Gaussian 16, Rev. B.01, Gaussian, Inc., Wallingford, CT, 2016.
[48] Y. Zhao, D.G. Truhlar, The M06 suite of density functionals for main group thermochemistry, thermochemical kinetics, noncovalent interactions, excited states, and transition elements: two new functionals and systematic testing of four M06-class functionals and 12 other function, Theor. Chem. Acc. 120 (2008) 215–241, https://doi.org/10.1007/s00214-007-0310-x.
[49] G.B. Damas. Atomic Scale Modelling in Photoelectrocatalysis: towards the Development of Efficient Materials for Solar Fuel Production, Acta Universitatis Upsaliensis, Uppsala, 2020, p. 86.
[50] P. Guiglion, C. Butchosa, M.A. Zwijnenburg, Polymer photocatalysts for water splitting: insights from computational modeling, Macromol. Chem. Phys. 217 (3) (2016) 344–353, https://doi.org/10.1002/macp.201500432.
[51] P. Guiglion, C. Butchosa, M.A. Zwijnenburg, Polymeric watersplitting photocatalysts; A computational perspective on the water oxidation conundrum, J. Mater. Chem. 2 (2014) 11996–12004, https://doi.org/10.1039/c4ta02044h.
[52] J.-L. Bredas, Mind the gap!, Mater. Horiz. 1 (2014) 17–19, https://doi.org/10.1039/C3MH00098B.
[53] J. Tomasi, B. Mennucci, R. Cammi, Quantum mechanical continuum solvation models, Chem. Rev. 105 (2005) 2999–3093, https://doi.org/10.1021/cr9904009.
[54] M.J. et al Frisch, Gaussian 09, Revision D.01, Gaussian 09, Revis. D.01, 2009, https://doi.org/10.1159/000348293.
[55] F. Wang, N. Mohammadi, S.P. Best, D. Appadoo, C.T. Chantler, Dominance of eclipsed ferrocene conformer in solutions revealed by the IR spectra between 400 and 500 cm-1, Radiat, Phys. Chem. 188 (2021) 109590, https://doi.org/10.1016/j.radphyschem.2021.109590.
[56] L.H. Gan, Q. Chang, J. Zhou, Transformations and tautomeric equilibrium among different intermediates in proline-catalyzed reactions of aldehydes or ketones, Chin. J. Chem. Phys. 26 (2013) 54, https://doi.org/10.1063/1674-0068/26/01/54-60.
[57] R.S. Sprick, L. Wilbraham, Y. Bai, P. Guiglion, A. Monti, R. Clowes, A.I. Cooper, M. A. Zwijnenburg, Nitrogen containing linear poly(phenylene) derivatives for photocatalytic hydrogen evolution from water, Chem. Mater. 30 (16) (2018) 5733–5742, https://doi.org/10.1021/acs.chemmater.8b02501.
[58] Y. Pellegrin, F. Odobel, Sacrificial electron donor reagents for solar fuel production, Compt. Rendus Chem. 20 (2017) 283–295, https://doi.org/10.1016/j.crci.2015.11.026.
[59] Y. Huang, L. Li, X. Peng, J. Peng, Y. Cao, Solution processed small molecule bulk heterojunction organic photovoltaics based on a conjugated donor–acceptor porphyrin, J. Mater. Chem. 22 (2012) 21841–21844, https://doi.org/10.1039/C2JM34429G.
[60] A.W. Prentice, M.A. Zwijnenburg, The role of computational chemistry in discovering and understanding organic photocatalysts for renewable fuel synthesis, Adv. Energy Mater. 11 (29) (2021) 2100709, https://doi.org/10.1002/aenm.202100709.
[61] A.W. Prentice, M.A. Zwijnenburg, Hydrogen evolution by polymer photocatalysts: A possible photocatalytic cycle, Sustain. Energy Fuels 5 (2021) 2622–2632, https://doi.org/10.1039/d1se00059d.
[62] J. Greeley, T.F. Jaramillo, J. Bonde, I. Chorkendorff, J.K. Nørskov, Computational high-throughput screening of electrocatalytic materials for hydrogen evolution, Nat. Mater. 5 (2006) 909–913, https://doi.org/10.1038/nmat1752.
[63] J. Kosco, I. McCulloch, Residual Pd enables photocatalytic H2 evolution from conjugated polymers, ACS Energy Lett. 3 (2018) 2846–2850, https://doi.org/10.1021/acsenergylett.8b01853.
[64] J. Kosco, M. Sachs, R. Godin, M. Kirkus, L. Francas, M. Bidwell, M. Qureshi, D. Anjum, J.R. Durrant, I. McCulloch, The effect of residual palladium catalyst contamination on the photocatalytic hydrogen evolution activity of conjugated polymers, Adv. Energy Mater. 8 (34) (2018) 1802181, https://doi.org/10.1002/aenm.201802181.
[65] M. Axelsson, C.F.N. Marchiori, P. Huang, C. Moyses Araujo, H. Tian, Small organic molecule based on benzothiadiazole for electrocatalytic hydrogen production, J. Am. Chem. Soc. 143 (2021) 21229–21233, https://doi.org/10.1021/jacs.1c10600.